Biotechnology Reports 34 (2022) e00722

Contents lists available at ScienceDirect

Biotechnology Reports

journal homepage: www.elsevier.com/locate/btre

Green decoration of graphene oxide Nano sheets with gelatin and gum Arabic for targeted delivery of doxorubicin☆

Mohamed Hasanin [a], Nesrin Fouad Taha [b,*], Aya Rashad Abdou [b], Laila Hasanin Emara [b]

[a] Cellulose and Paper Department, Chemical Research Institute, National Research Centre, 33 EL Bohouth st. (former EL Tahrir st.), Dokki, Giza, P.O.12622 Egypt
[b] Medicinal and Pharmaceutical Chemistry Department, Pharmaceutical and Drug Industries Research Institute, National Research Centre, 33 EL Bohouth st. (former EL Tahrir st.), Dokki, Giza, P.O.12622 Egypt

ARTICLE INFO

Keywords:
Gelatin/gum arabic/graphene oxide tri-nanocomposite
Doxorubicin

ABSTRACT

Tri-nanocomposite system of biocompatible polymers (gelatin/gum arabic) functionalized onto graphene-oxide nanosheets for controlling the release of an anticancer, doxorubicin (DOX), was fabricated via green-biosynthesis. Biocompatibility and nano-size stability of the tri-nanocomposite was characterized by SEM, TEM, FTIR, XRD, and zeta-potential. Loading-efficiency, release-behavior and cytotoxic-activity of DOX-loaded-composite in WI-38 normal-lung-fibroblast and A549 lung-carcinoma cells were investigated. High DOX-loading (at pH 9.5), with pH-sensitive release from loaded-composite was achieved, with 25% and 77% DOX released, at physiological pH 7.4 and cancerous pH 5.3, respectively. Stability of tri-nanocomposite system was confirmed over 3-months storage at accelerated conditions, as presented by FTIR, XRD, TEM, zeta-potential and in-vitro release assays. High proliferative inhibitory effect of DOX loaded-composite, on A549-cells, with minimal toxicity on WI-38-cells, with IC_{50} values of 51.9 ± 0.46 and 185±1.08 μg/mL, against A549 and WI-38, respectively. Proposed tri-nanocomposite offers a novel combination of gelatin/gum arabic with graphene-oxide for targeted drug-delivery and efficient anti-cancer therapy.

Introduction

Chemotherapeutics are commonly used for curing different types of cancer by targeting the fast-growing cancer cells [1]. However, due to the non-specific nature of anti-cancer drugs, they might attack those healthy cells as well, resulting in the failure of conventional chemo-therapy. The lack of selectivity of common anti-cancer drugs lead to their most common side effects including; hair loss, vomiting, fatigue and the risk of developing various infections [2]. In addition, multi drug resistance is a main complication to effective chemotherapy, where cancer cells develop resistance against cytotoxic drugs during or shortly after commencement of therapy [3]. All these demerits associated with chemotherapeutics extremely limit the development of new anticancer drugs [4].

Consequently, providing innovative drug delivery systems with novel drug carriers for the already available anti-cancer drugs, with effective drug loading, is quite essential for targeting drug release into the tumor environment [4–6]. Among the recent potential delivery carriers are; polymeric particles [7], nanomaterials, microspheres [8], dendrimers [9], liposomes [10], and carbon nanotubes [2]. Nano-carriers allow the adjustment of drug release rate, alter drug distribution in vivo, and enhance drug efficiency through encapsulation and ab-sorption [2, 11].

Carbon based nano-materials including graphene oxide (GO) have been considered as the most advanced vehicles for efficient delivery of drugs and biomolecules [4, 12]. GO is a vehicle with good biocompat-ibility, high surface area, low cost as well as high drug loading capacity among other drug carrier groups [13]. GO exhibit large numerous functional groups such as epoxy, hydroxyl and carboxyl groups [4]. GO exhibits a p-conjugated structure, where efficient loading of drugs onto GO nano sheets occurs by π-π stacking and van de Waals forces [4]. GO has been used as an excellent nanocarrier for various model drugs, for example ibuprofen and amoxicillin [14], heparin [15], 5-fluorouracil [16], and doxorubicin [17].

Yet, major shortcomings of using GO for drug delivery is the presence of craggy edges which might lead to the disruption of normal cells and its possible aggregation on cell membranes resulting in its cellular toxicity [18]. To overcome such limitations, GO nanoparticles are often

☆ This research did not receive any specific grant from funding agencies in the public, commercial, or not-for-profit sectors.
* Corresponding author.
E-mail address: nesrintaha77@gmail.com (N.F. Taha).

https://doi.org/10.1016/j.btre.2022.e00722
Received 16 February 2022; Received in revised form 9 March 2022; Accepted 16 March 2022
Available online 18 March 2022

functionalized, through chemical or physical attachment, with biocompatible polymers, to reduce its cytotoxicity, enhance its solution solubility as well as its stability under physiological conditions [18]. Polysaccharides based-nanomaterials have been developed as drug delivery vehicles, owning to their high stability, biodegradability, low toxicity, and biocompatibility. Gelatin, gum Arabic, starch, chitosan, cellulose, glycogen polyethylene glycol, poly-caprolactone, polylactic acid and polyvinylpyrrolidone are examples of the most known polymers functionalized onto GO sheets [19–21].

Gelatin (GL), a natural macromolecule, is generally used in various fields including food and medicine. GL offers characteristic membrane-forming ability, biocompatibility, and non-toxicity [22, 23]. Immobilization of GL on graphene surface occurs via hydrophobic–hydrophobic interactions, hence enhancing the stability of graphene dispersion [22]. GO acts as both an effective reinforcement filler and a biological activator in hydrophilic biopolymers such as GL, offering the biopolymer–GO nanocomposites great potential to be further developed in biomedical fields [24].

In addition, Gum Arabic (GA) is a natural tree gum exudate that has a complex polysaccharide structure and is well known for its biodegradability, biocompatibility and water solubility [25]. GA remarkable rheological and emulsifying properties play critical role in stabilization of GO [26], while its highly branched structure offers multiple carboxyl (–COOH) and hydroxyl (–OH) groups for attachment with various drugs [27, 28]. High solubility of GA in acidic medium (pH 4–5) and its milder in highly alkaline solution (pH $>$ 7) plays a crucial role as a drug delivery vehicle. Few reports of the use of GA as stabilizer for nanoparticles are available [29, 30].

In this context, the thermodynamic compatibility of water-soluble polysaccharides according to the Flory-Huggins interaction parameter is a fundamental aspect to understand, to predict possible interaction with cellular components [31–34]. Herein, the thermodynamic incompatibility between polysaccharides and cellular proteins should be figured out to ensure that the polysaccharides drug carrier system will deliver drug to its target site, without any side reaction affecting drug activity [35].

Doxorubicin (DOX) is a commonly known first-line treatment for various pathological conditions such as breast and lung cancers and multiple myeloma. DOX recognized adverse side effects; include cardiotoxicity, nephrotoxicity, alopecia, vomiting, leukopenia, and stomatitis [18]. Also, intravenous administration of DOX is quite difficult as a result of its low solubility in aqueous media [2]. DOX kills cells by preventing DNA replication and subsequent cell division [36]. Accordingly, DOX operates when it is adequately transported into the nucleus of cancerous cells. Nevertheless, most of the well-recognized drug carriers like liposomes and nanoparticles fail to migrate to the cellular nucleus because of their large size, and hence affect the sufficient release of their cargoes in the cytoplasm [37]. Thus, exploiting novel nano-carrier fundamental ability in protecting DOX from degradation, prolonging its circulation lifetime, reducing its dose, with subsequent positive impact on its bio-distribution and pharmacokinetics is highly recommended [38].

A few studies discussed efficient loading of anti-cancer drugs onto GO nanosheets, in the presence of either GL [24] or GA [39] as bioactive polymers. Yet, so far, no available data discussed combining both characteristic functions of GL and GA for green decoration of GO nanosheets. Herein, we developed a simple approach for the functionalization of both GL and GA onto GO nanosheets, which open new opportunities for novel biopolymer based - GO composite in a wide range of potential applications.

The aim of the present study was the preparation of a novel green biocompatible nontoxic, GL-GA-GO tri-nanocomposite for loading DOX. Characterization of unloaded and DOX loaded tri-nanocomposites via scanning electron microscope (SEM), transmission electron microscopy (TEM), Fourier-transform infrared (FTIR), ultra violet-visible (UV–Vis), X-ray diffraction (XRD) and zeta potential analyses was conducted. In addition, evaluation of drug loading efficiency, in-vitro release at different pHs and accelerated stability studies for DOX/GL-GA-GO composites were carried-out. Cytotoxicity and therapeutic efficiency assays in normal and cancer human lung cell lines were included.

Materials and methods

Materials

Doxorubicin hydrochloride (DOX) was purchased from Sigma-Aldrich. Graphite powder was purchased from Shanghai Yifan Graphite Co, China. Gelatin Bovine-B (GL) and Gum Arabic (GA) were obtained from Sigma Aldrich, USA. Other chemicals and reagents employed in the study were of analytical grade. Milli-Q purified water (Millipore Corp., Billerica, MA, USA) was used for the preparation of buffers and dissolution media.

Dimethyl sulfoxide (DMSO) was obtained from Loba Chemie, India. Human cell lines used namely; WI-38 (normal fibroblasts derived from lung tissue) and A549 (lung carcinoma) were obtained from "The Regional centre of Mycology and Biotechnology"- Al-Azhar University, Egypt. MTT "3-(4,5-dimethylth¬iazol-2-yl)−2,5-diphenyltetrazolium-bromide" was acquired from Bio-basic, France. Griess reagent was acquired from Sigma-Aldrich, USA.

Methods

Graphene oxide (GO) synthesis

GO was prepared according to hummer`s method with minor modification [40]. Sulphuric acid and phosphoric acid were mixed and stirred for 5 min in a ratio of 9:1. Addition of graphite powder (0.225 g) to 30 mL of mixed acids solution was carried out, under stirring condition. Followed by slow addition of 1.32 g potassium permanganate and mixture was continuously stirred for 6 h till the solution change into dark green. For the removal of excess potassium permanganate, hydrogen peroxide (0.675 mL) was slowly added, with stirring for 10 min. GO washing was carried out using 12% hydrochloric acid for three times followed by five times washing with distilled water. GO was dried overnight using vacuum oven at 105 °C.

Preparation of GL-GA-GO tri-nanocomposite

Tri-nanocomposite was prepared via a green synthesis method as follows; equal weights (1 g) of both gelatin (GL) and gum arabic (GA) were dispersed in 100 mL distilled water using mechanical homogenizer. On the other side, 0.01 g of GO was dispersed in distilled water and homogenized by an ultra-sonication prop for 10 min (Ultrasonic Processors Vc 505, USA). The previously prepared solutions were mixed under magnetic stirring at 1500 rpm for 1 h at 70 °C.

DOX loading onto the GL-GA-GO composite

The loading of DOX was carried out as follows; an aqueous DOX solution (10 mL) was dispersed in 10 mL of tri-nanocomposite. 0.1 M of HCl or NaOH solution was added for adjusting pH of the mixture in ranges of 5.5 till 9.5 [4]. The homogeneous mixture was shaken (temperature-controlled shaking water-bath, Lab-Line, USA) overnight at 25 °C for successful DOX loading onto the GL-GA-GO tri-nanocomposite. Collection of loaded composites (denoted as DOX/GL-GA-GO) was done after several centrifugation (9000 rpm) and washing with water with the same pH value till the supernatant became colourless [4]. Collection of supernatants was done and free DOX was calculated via UV–VIS spectrometry at 480 nm. The final purified DOX/GL-GA-GO composites were freeze-dried and stored at −20 °C in dark before use. With the purpose of optimizing DOX loading, actual DOX concentration was changed from 0.25 to 2.5 mg/mL, at pH condition of 9.5.

Actual DOX loading and loading efficiency were evaluated according to the following equations:

$$\text{Actual DOX loading\%} = \text{Mt/Mc x100\%} \quad (1)$$

$$\text{DOX loading efficiency\%} = \text{Mt/Mox100\%} \quad (2)$$

Mt, Mc, and Mo signify the mass of DOX loaded onto GL-GA-GO tri-nanocomposite, GL-GA-GO tri-composite and initial DOX used, respectively.

Characterization of DOX /GL-GA-GO tri-nanocomposite

SEM. The surface of the prepared tri-nanocomposites was inspected using field emission scanning electron microscope (FE-SEM), with energy dispersive X-ray analysis (EDX) [Model Quanta 250, FEG (Field Emission Gun); Netherlands], with accelerating voltage 30 KV.

TEM. Transmission electron microscopy (TEM) coupled with selective area electron diffraction (SAED) (Model JEM2010, Japan) were used to investigate particle size and morphology of unloaded and DOX loaded GL-GA-GO tri-nanocomposites. Particle size distribution of DOX loaded composite analysed by TEM ImageJ processing software.

FTIR. Structural changes of studied samples were investigated by Fourier-transform infrared (ATR-FTIR) spectroscopy "Spectrum Two IR Spectrometer - PerkinElmer, Inc., Shelton, USA". Spectral analysis was obtained by 32 scans and 4 cm^{-1} resolutions in wavenumbers ranging from 4000 to 400 cm^{-1}. The analysis was performed in triplicate.

XRD. The crystal structure of the prepared tri-nanocomposite was determined using an X- ray diffraction (XRD) "Model diffractometer, Shimadzu 7000, Japan, Cu-Kα radiation (λ = 0.15418 nm, and Ni filter". XRD diffractometer was run at 40 kV and 40 mA over a 2θ range of 10°−70° The analysis was performed in triplicate.

UV–Vis. UV-Visible spectrophotometric analysis of plain DOX, GO, prepared GL-GA-GO tri-nanocomposite and DOX loaded composite (DOX/GL-GA-GO) was done in the range of 200–800 nm (DU–650 UV–Vis spectrophotometer, Beckman, USA). The analysis was performed in triplicate.

Zeta potential. Dynamic light scattering "DLS, Malvern Instruments Zetasizer Nano-ZS instrument, UK" was used to examine the zeta potential of different samples in aqueous media. The analysis was performed in triplicate.

Colloidal stability of GL-GA-GO tri-nanocomposite

The stability of the formed GL-GA-GO nano-colloid compared to plain GO was investigated by incubation in distilled water, physiological pH of 7.4 as well as acidic tumor pH of 5.3 for several hours. Colloidal stability was then visually inspected.

DOX release from tri-nanocomposite

Release tests

DOX loaded GL-GA-GO composites (2 mg) dispersed in phosphate buffer saline (PBS) [2 mL, 40 mM, at two pH; 7.4 (physiological pH) and 5.3 (endosomal pH of cancer cells)] were placed in a dialysis bag (Seamless Cellulose Tubing, MWCO 12,000 – 14,000, width of 34 mm, diameter of 21 mm, thickness of 23 μm, pore diameter of ca. 25Å, LOT No.: 21,057, Viskase Sales Corp.) and dialyzed against the corresponding buffer medium (13 mL). An equivalent amount of plain DOX was in vitro evaluated for comparison [41]. Incubation of all samples for the release study was done in a temperature-controlled shaking water-bath (Lab-Line, USA) at 37 °C with shaking at 90 rpm. The release study was done in triplicates. At specified time intervals (0.5, 1, 2, 3, 4, 24 and 48 h), release samples (2 mL) were withdrawn and DOX concentration was quantified by UV–Vis spectral method at 480 nm. The outer buffer medium was kept constant by replenishing with equal volume of buffer solution.

Release data analysis

The in vitro release data of DOX loaded GL-GA-GO tri-nanocomposite was incorporated into various release kinetic models and the corresponding mathematical equations were applied: zero-order (Eq. (3)) [42, 43], first-order (Eq. (4)) [42–44] and Higuchi square root of time (Eq. (5)) [42, 44] release models, as well as the use of the Korsmeyer – Peppas model (Eq. (6)) to describe the possible mechanism of drug release [45]. The selection of the most appropriate model was dependent on the highest value of correlation coefficient (R2).

$$\text{Mt/M}\infty = \text{M0} + \text{k0xt} \quad (3)$$

$$\ln(100 - \text{Mt}) = \ln 100 - \text{k1xt} \quad (4)$$

$$\text{Mt/M}\infty = \text{M0} + \text{kH xt1/2} \quad (5)$$

$$\log(\text{Mt / M}\infty) = \log\text{kKP} + \text{nxlogt} \quad (6)$$

where M0, Mt, and M∞ are the amount of drug dissolved at the beginning, at time t, and the total mass of drug dissolved at an infinite time, respectively. The coefficients ko, k1, kH, and KKP signify the zero-order, first-order, Higuchi, and Korsmeyer - Peppas's rate constants, respectively. While n stands for diffusional exponent of the Korsmeyer - Peppas model.

Storage stability of DOX-GL-GA-GO tri-nanocomposite

The prepared DOX loaded tri-nanocomposite was stored in a stability chamber of 40 °C ± 0.5 °C and relative humidity of 75% for 3 months. The stored samples were re-evaluated against fresh samples, using FTIR, XRD, TEM, zeta potential and in vitro release assays.

Cytotoxicity evaluation

Cell culture

The cytotoxicity of plain DOX, unloaded and DOX loaded GL/GA/GO tri-nanocomposite were studied in human WI-38 (normal fibroblasts derived from lung tissue) and human A549 (lung carcinoma) cell lines. Initially, cells were incubated in 96-well plates at density equals to 1×10^4 cells/well. Cells were inoculated in DMEM in the presence of: high glucose (4500 mg/L), L-Glutamine (4 mM/L), supplemented with heat-deactivated fetal bovine serum (10%), penicillin (10,000 U/mL), and streptomycin (10,000 μg/mL). Cells were permitted to adhere for 24 h till about 80%–90% confluence.

Cell viability assay

Evaluation of cellular viability was carried out by MTT assay in triplicate. Yellow MTT "3-(4,5-Dimethylthiazol-2-yl) −2, 5- diphenyltetrazolium bromide, a tetrazole" was reduced to purple formazan in living cells' mitochondria [46].

WI-38 and A549 cells were seeded in 96-well plates at 5 × 105/mL, followed by incubation at 37°C and 5% CO2 for 24 h. After acceptable cell growth, different concentrations of plain DOX, unloaded and drug loaded tri-nanocomposite in fresh maintenance medium were added and incubated at 37°C for 24 h.

Later, test solution was replaced with MTT solution for 4 h. Absorbance was measured (570 nm) by ELISA Reader system "Sun Rise TECAN, Inc., USA". Treated cells, stained with 0.25% crystal violet, were studied for morphological changes under inverted microscope "CKX41; Olympus, Japan" coupled with digital microscope camera [47].

Data calculations

The percentage cell viability was calculated according to the

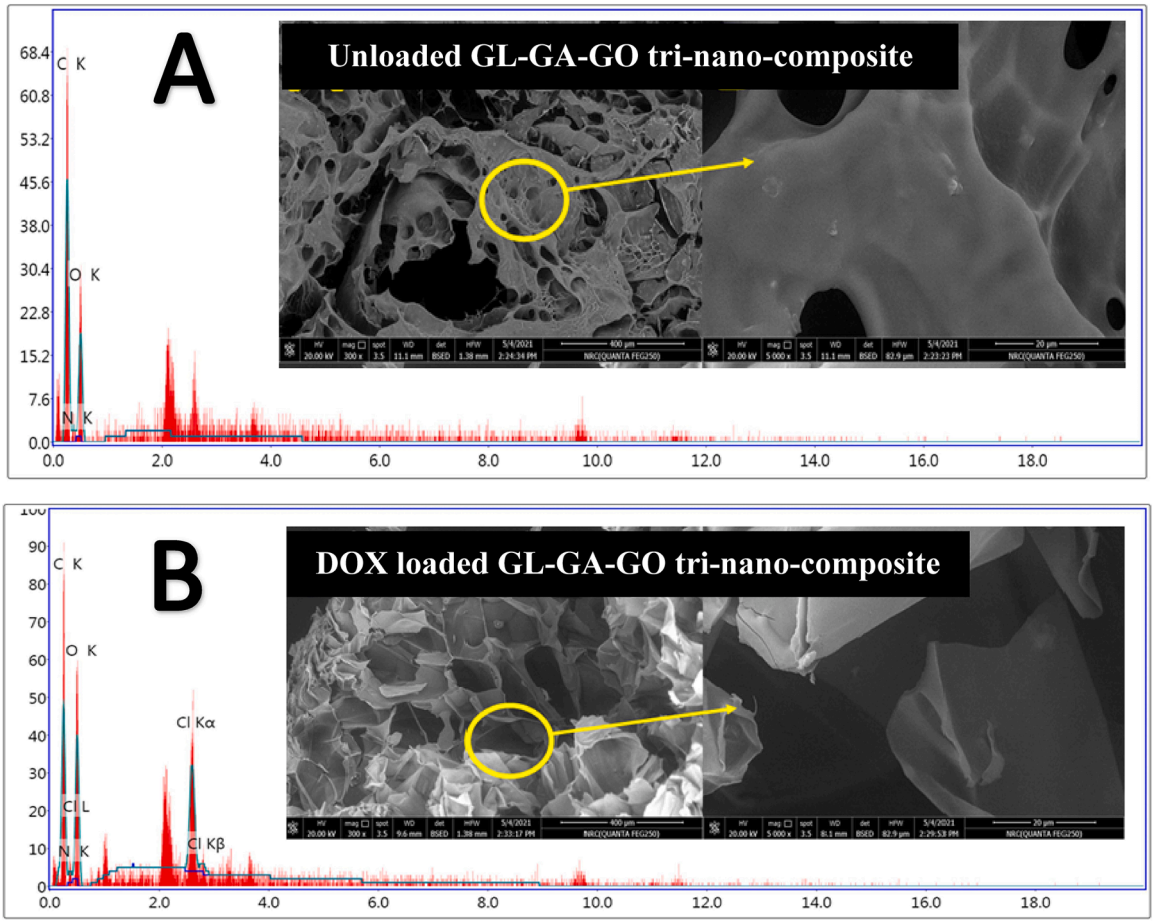

Fig. 1. SEM images and EDX charts of unloaded and DOX loaded tri-nanocomposite.

following equation [48]:

$$\text{Cell viability percentage} = (\text{ODt} / \text{ODc}) \times 100\% \quad (7)$$

ODt and ODc represent mean optical density of test-treated cells and untreated, control cells, respectively.

The 50% inhibitory concentration (IC50) was calculated (the concentration of a single compound causing 50% cell death) [49], where values were expressed as mean ± standard deviation ($n = 3$).

Results and discussion

Characterization of the tri-nanocomposite

SEM & TEM

Surface features of the prepared tri-nanocomposite as well as the morphological changes occurring after drug loading were presented by SEM (Fig. 1) and TEM images (Fig. 2). EDX analysis was carried out to detect changes in elemental compositions of unloaded and DOX loaded composite (Fig. 1).

SEM images of unloaded GL-GA-GO tri-nanocomposite showed a smooth spongy-like surface with numerous, clear integrated holes (Fig. 1a), with the close-up SEM image confirming typical GO sheets appearance with small size flake-like structures (Fig. 1a).

On the other hand, DOX loaded nanocomposite represented a rough, wrinkled- surface (Fig. 1b). Moreover, the porous structure of GL-GA-GO nanocomposite was retained, with a collapsed 3D network of polysaccharide as a result of the π–π stacking bond between the aromatic ring of DOX and nanocomposite sheets [2].

In this context, the EDX chart of unloaded tri-nanocomposite presented relative atomic percentages of the following elements: carbon (46.59%), oxygen (38.45%) and nitrogen (14.97%) (Fig. 1a), which are constituent elements of GO sheets [50]. While, EDX chart of DOX loaded nanocomposite (Fig. 1b), illustrated the appearance of chlorine (5.62%) as well as an increase in oxygen atomic ratio (40.7%) as a result of DOX loading (molecular formula of DOX.HCl; C27H29NO11.HCl) [51].

TEM micrographs presented in Figure (2a,b), confirmed the nanostructure of unloaded composite, based on GO typical sheet structure morphology, with some dark patches present on the surface, describing successful functionalization process [52]. Moreover, porous surface was clearly observed in both unloaded (Fig. 2a,b) and drug loaded (Fig. 2c, d) nanocomposites. However, DOX loaded nanocomposite showed a compacted structure over the GO sheets, emphasizing the electrostatic interaction between DOX and nanocomposite. Additionally, SAED illustrated the changes in the intermolecular structure of nanocomposite before and after DOX loading. Where, a typical, single, well-defined array of hexagonal diffraction pattern was observed for the unloaded composite (Fig. 2e), whilst in DOX loaded composite, multiple, sharp spots were visible (Fig. 2f) [53]. Size distribution of the prepared loaded tri-nanocomposite, confirmed its presence in the nano size range of 15 – 55 nm (average size of 35 nm) (Fig. 2g).

FTIR

Proper design of an efficient new drug carrier system critically depends on the interaction between the system component/s. FTIR spectra of plain GO, GL, GA, DOX forms as well as the prepared GL/GA/GO and drug loaded composites were observed in Fig. 3a,b. GO spectrum confirmed typical bands at 1715, 1616, 1412 and 1061 cm-1, assigned for C = O stretching, O–H stretching, O–H deformation and –O–O–H stretching, respectively [54]. GA spectrum showed significant bands at

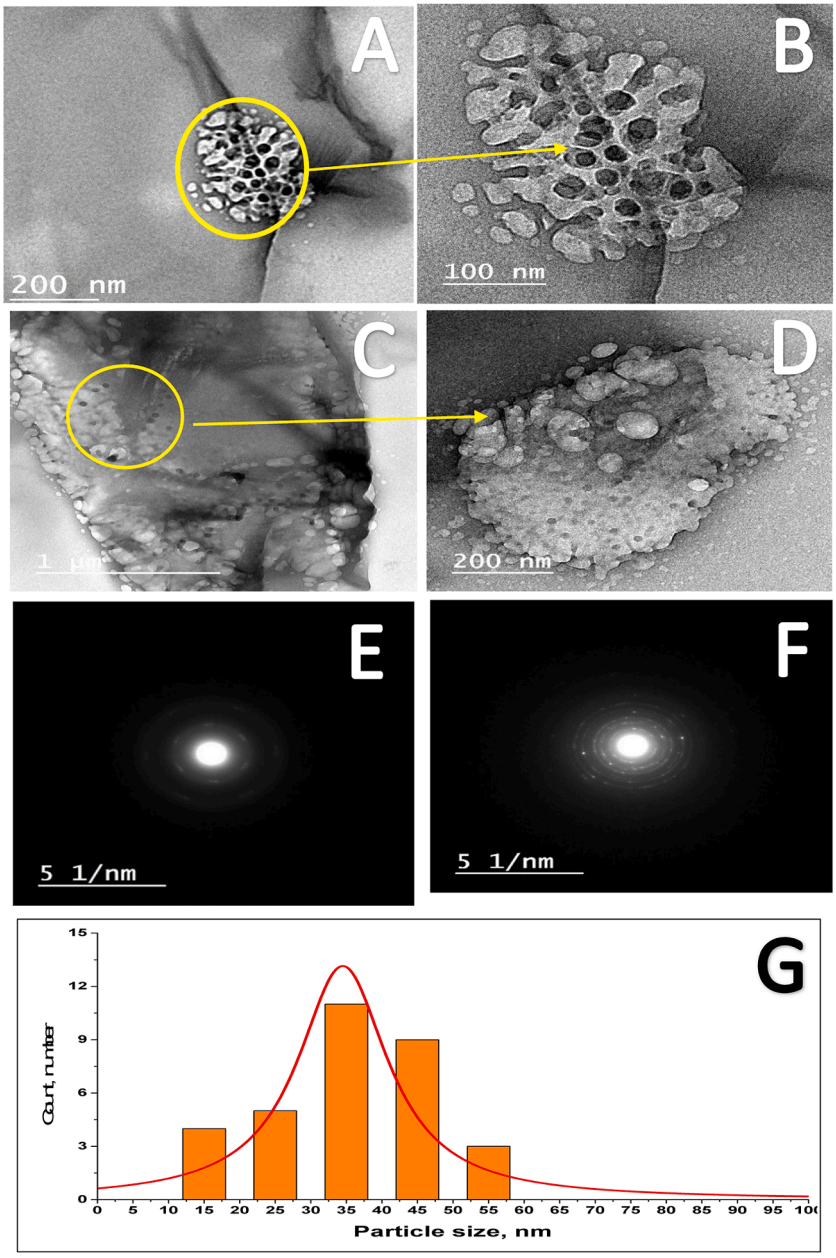

Fig. 2. TEM images of unloaded (A, B) and DOX loaded (C, D) tri-nanocomposite. SAED pattern of unloaded (E) and DOX loaded composite (F).; Particle size distribution analysed by TEM ImageJ processing software (G).

3308 (O–H stretching vibration), 2933 (C–H stretching of CH2 group), 1602 (COOH stretching), 1429 (uronic acid (COOH)), 1018 – 825 (linkage of polysaccharide) and 775 cm-1 (1– 4 linkage of galactose and 1– 6 linkage of mannose) [55]. GL showed characteristic bands at 3454, 2925, 1703, 1229 and 1031 cm−1, which were attributed to overlapping of NH and OH bond stretching vibration, COOH group stretching vibrations, C = O stretching, NH bending vibration of the amide group and C–O–C of the amide bond in gelatin stretching vibrations, respectively [56].

FTIR spectrum of plain DOX confirmed the characteristics bands at 3567, 2960, 2863, 1726, 1579, 1070, 871 and 652 cm−1 for N–H stretch, C–H stretch, CH2 stretching, C = O stretch, C = C ring stretch, C–O–C stretch, C = H bend and C = C ring bend, respectively (Fig. 3a) [57].

As observed in Fig. 3b; FTIR spectrum of unloaded GL-GA-GO composite showed that the characteristic surface functional groups of all components were attained with minor shifting. Also, new bands, not recorded in native nanocomposite components, were assigned corresponding to O–H stretching vibration at 3292cm-1, C–H stretch at 2944 cm-1 and C = O stretching at 1648 cm-1, indicative of the successful formation of the tri-nanocomposite [15].

For DOX/GL-GA-GO composite spectrum (Fig. 3b); DOX main characteristic bands were clearly present, indicating productive loading of drug onto the composite system. However, the loading of DOX onto the tri-nanocomposite resulted in appearance of new bands corresponding to the high content of free CH groups at 2831 cm-1, C = C ring stretch at 1339 - 1238 cm-1 as well as C–O–C stretch at 1085 cm-1 (Fig. 3b).

XRD

The crystallography of plain drug, plain components of tri-nanocomposite as well drug composite system was presented in Fig. 3c,d. GO showed a strong and sharp peak at 10.8°, unlike the reported main peak of graphite at 26.6° [58]. GA pattern exhibited peaks

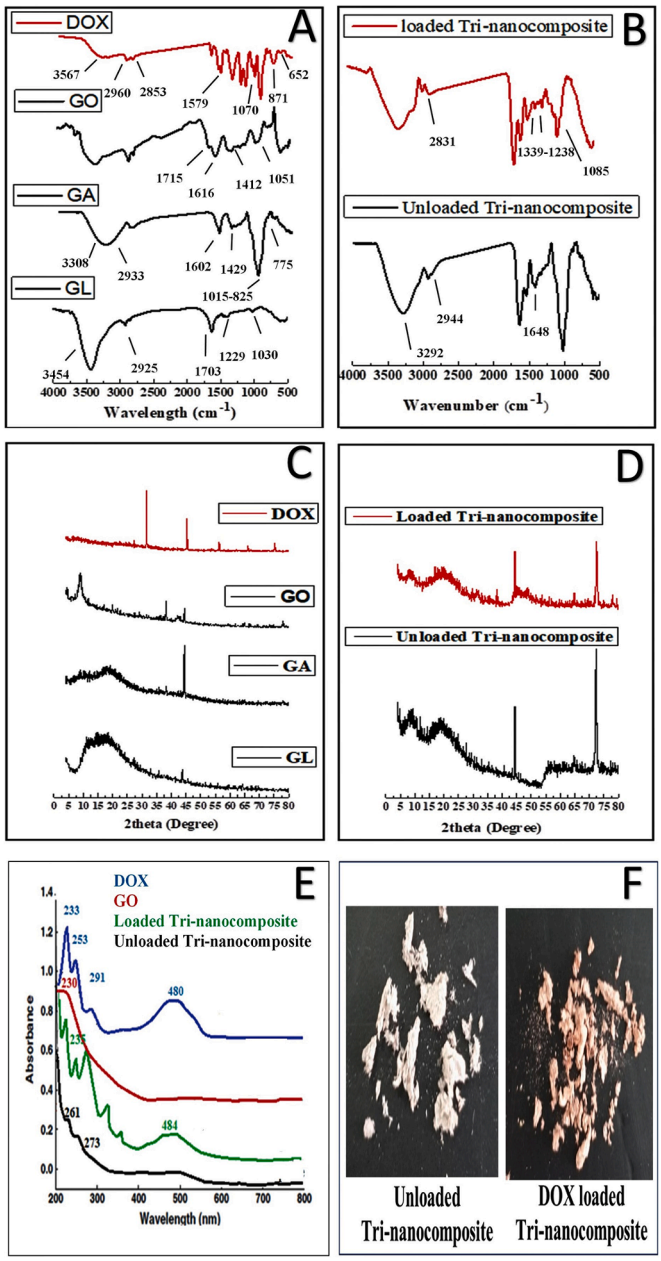

Fig. 3. FTIR (A, B); XRD patterns (C, D); and UV Spectra (E) of the prepared unloaded and DOX loaded tri-nanocomposite with their respective plain components. photographs confirming color change of the unloaded tri-nanocomposite from dark brown to red as a result of drug loading (F).

at 18.7° and 42.3°, predictable for amorphous gum arabic [59]. GL exhibited prominent broad peak at around 18o-22o characteristic to the amorphous structure of all gelatines [60]. In addition, XRD pattern of plain DOX exhibited sharp peaks at scattered angles, confirming drug crystalline nature [61].

On the contrary, XRD pattern of the unloaded tri-nanocomposite showed the disappearance of GO characteristic band at 10.8° (Fig. 3d), indicative of the loss of the original lamellar structure and the presence of sheets in disordered arrays [62,63]. Whereas, most of DOX crystalline peaks were not present in loaded composite suggesting the existence of DOX in an amorphous form in the GL-GA-GO structure (Fig. 3d).

UV–Vis

The formation of DOX loaded GL-GA-GO tri-nanocomposite was confirmed by UV–Vis spectra in UV range of 200–800 nm (Fig. 3e). Meanwhile, photographs in Fig. 3f, confirmed color change of the tri-nanocomposite from dark brown to red before and after drug loading, respectively. GO showed a broad absorption peak at 230 nm, related to π→π transition of electrons concerned with aromatic rings [51], while, GO-GL-GA composite showed the appearance of absorption peaks at 261 and 273 nm (Fig. 3e). Absorption peaks of plain DOX were observed at 233, 253, 291 and 480 nm [64]. Conjugation of DOX with nanocomposite of GO-GL-GA resulted in slight shift of DOX peaks towards longer waves at 235 and 484 nm indicating successful immobilization of DOX onto the nanocomposite through π→π stacking (cf. photographs presented in Fig. 3f).

Zeta-potential

Zeta potential measurement is an important tool to evaluate the system stability during the studding of appropriate nanocomposite as a drug carrier system. Zeta potential of plain GO, prepared tri-nanocomposite and DOX loaded composite was calculated. As, reported by Zhang et al., differences observed in zeta potential values, indirectly suggest successful functionalization of polymers onto the GO nanosheets [15]. In the present study, zeta potential of GO was −24.76 ±0.6 mV, which is due to presence of large number of hydroxyl, carbonyl and epoxy groups on GO surface [15]. The unloaded tri-nanocomposite offered acceptable zeta potential value in negative region (−9.7 ± 1.2 mV), while loading of DOX onto the tri-nanocomposite resulted in an increase of zeta potential (17±1.2 mV). Positively charged DOX loaded composite ensured system stability as well as promote beneficial connection between the prepared delivery system and negative-charged cell membrane via electrostatic adsorption [65].

Colloidal stability of GL-GA-GO tri-nanocomposite

The Colloidal stability of the prepared GL-GA-GO tri-nanocomposite was investigated, against pure GO, in distilled water, physiological pH of 7.4 as well as acidic tumor pH of 5.3, and results were presented in Fig. 4. Results showed that GO was stable in water but aggregated in physiological and acidic environment (Fig. 4), as previously reported [15]. On the other hand, GL-GA-GO tri-nanocomposite allowed excellent dispersibility at studied pHs for several hours (Fig. 4).

Based on the current characterization results, it could be concluded that functionalizing of GL, GA onto GO sheets improved GO physical stability, as confirmed by TEM, zeta potential and colloidal stability in different media.

DOX loading onto GL-GA-GO tri-nanocomposite

The amount of DOX loaded onto the nanocomposite was quantified according to the standard curve constructed of DOX concentration versus its absorbance at 480 nm [64] (Fig. 5a).

DOX exhibits a pH-dependent hydrophilicity characteristics, where in acidic pH environment, protonation of DOX occurs rendering it as water-soluble, which does not provide an ideal condition for hydrophobic π–π stacking interaction with the GL-GA-GO nanocomposite. On the other hand, in basic environment, DOX is present in a de-protonated form, which is quite hydrophobic, hence allowing effective bonding with the nanocomposite [66,67].

Loading of DOX onto the GL-GA-GO nanocomposite were studied at different pHs ranging from 5.5 till 9.5 pHs (at fixed ratios of DOX: GL-GA-GO of 1:1) and results were presented in Fig. 5c. Changing pH from acidic to alkaline side, led to an increase in the loading amount of DOX. Where, highest actual DOX loading and loading efficiency values

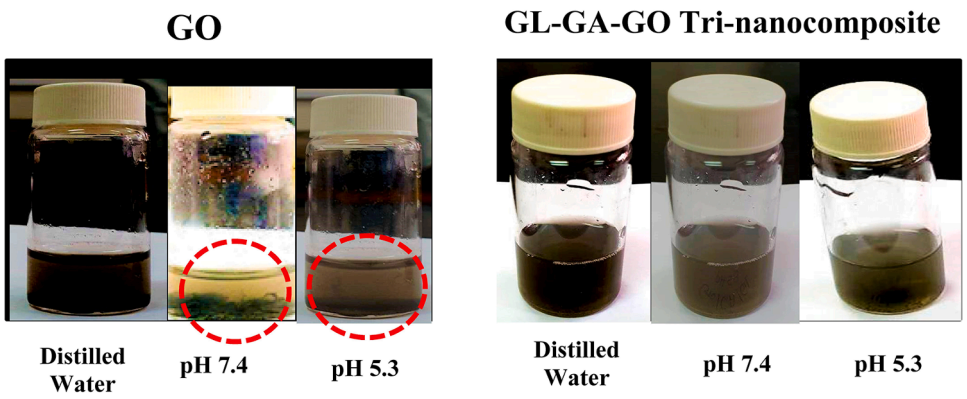

Fig. 4. stability of synthesized GL-GA-GO tri-nanocomposite against GO in different media.

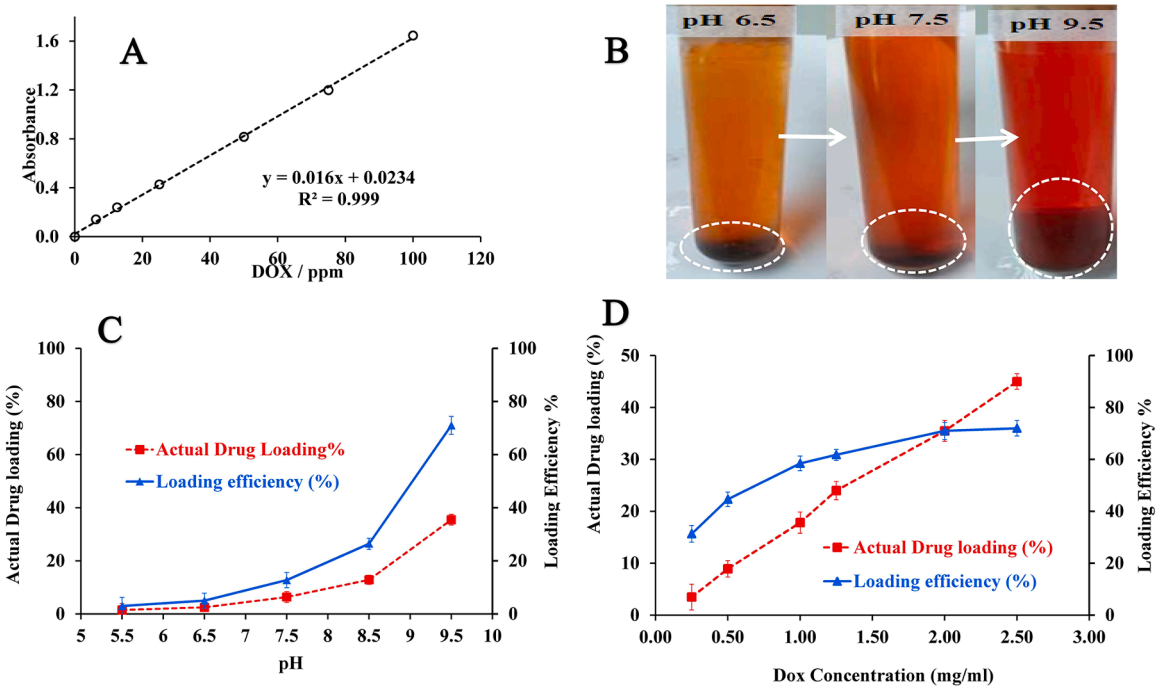

Fig. 5. Calibration curve of plain DOX at 480 nm (A); with images showing effect of pH on DOX loading from the composites (B); actual loading and loading efficiency percentages of DOX onto GL/GA/GO tri-nanocomposite at: different pHs (C); different DOX concentrations (D) (mean± SD, $n = 3$).

of 35.5 and 71.8% were observed, respectively, at pH 9.5 (Fig. 5c).

As presented in Fig. 5b; at pH 6.5; loading of DOX was incomplete, with yellowish red supernatant and a partial hydrocolloid mass. On the other hand, further increase in pH to more alkaline side; enhanced the red color of supernatant with gradual increase in colloidal mass, indicating higher loading of DOX onto the tri-nanocomposite.

Although, previous studies were carried out to explore pH adjustment for efficient DOX loading onto GO sheets [4,15,68]. Yet, controversial results regarding pH optimization have been described. Whereas some studies reported maximum DOX loading onto GO, occurred at neutral pH [62]. Others confirmed basic pH as optimal for better DOX loading [4,15]. These varying results might be associated with changing the type of polymer employed for conjugation onto GO sheets.

At optimal pH condition of pH 9.5, actual DOX loading and loading efficiency percentages onto the GL-GA-GO nanocomposite were further optimized by ranging DOX concentrations from 0.25 to 2.5 mg/mL (Fig. 5d). It was clearly observed from Fig. 5d that increasing DOX concentrations from 0.25 to 2 mg/mL led to simultaneous increase in both drug loading and loading efficiency. Yet, further increase of DOX concentration to 2.5 mg/mL led to subsequent increase in actual drug loading of 45% with no further increase in loading efficiency (~ 73%). Herein, adjusting both DOX and GL-GA-GO nanocomposite concentrations at 2 mg/mL each, allowed optimum DOX loading percentage and efficiency. On the other hand, a previous study by Yang et al. 2008, confirmed successful loading of DOX on GO at a value of 2.35 mg/mg, with initial DOX concentration of 0.47 mg/mL [68].

Such differences reported, regarding factors influencing loading capacity of DOX onto GO might be associated with changing the type of polymer employed for conjugation onto GO sheets. As clearly presented in the current study, functionalization of GL and GA onto GO nanosheets, allowed successful DOX loading onto GL-GA-GO nanosheets, with loading efficiency $\geq$ 70%, at optimum conditions of pH 9.5 and equal ratios of DOX and tri-nanocomposite.

DOX release from GL-GA-GO nanocomposite

Fig. 6a presented the in vitro release of DOX from GL-GA-GO composite at two different pHs conditions; i.e., pH 5.3, representing acidic tumor site as well as pH 7.4, representing the physiological environment, for 48 h.

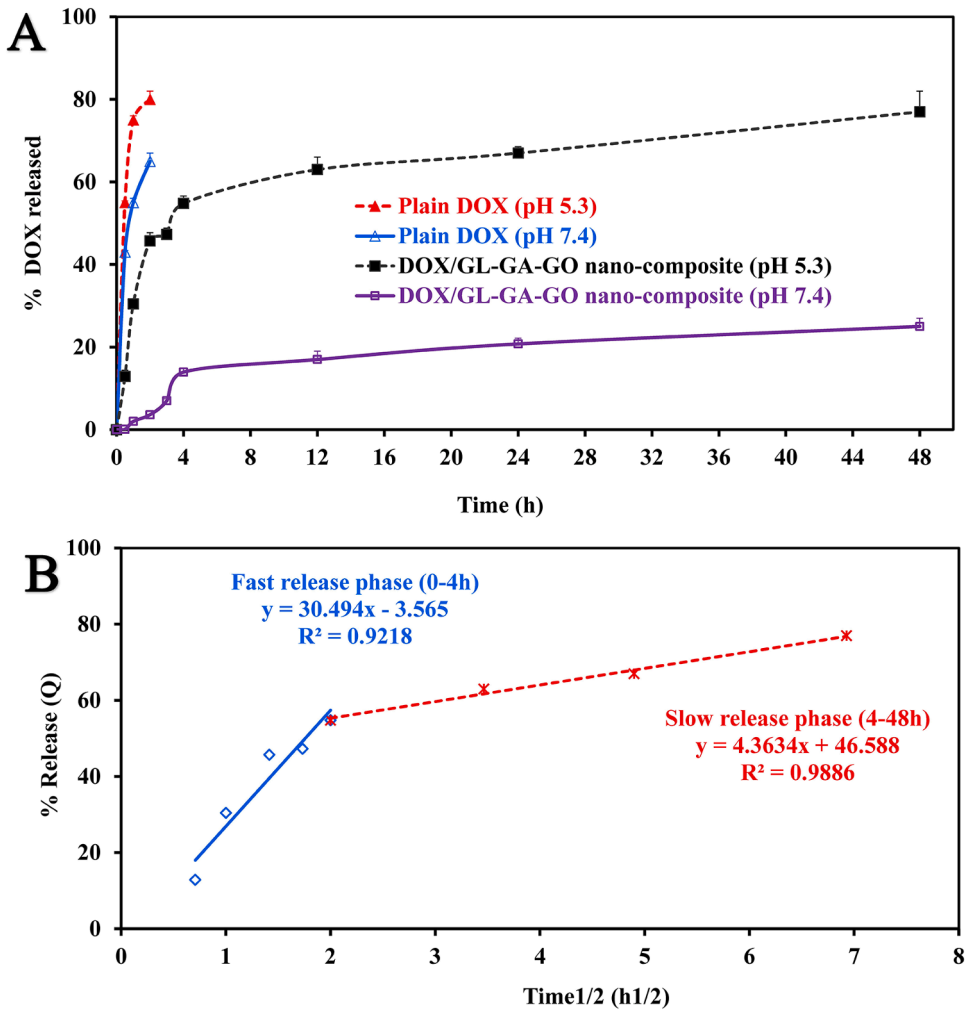

Fig. 6. Release pattern (A) and corresponding release kinetics (B) of DOX loaded GL/GA/GO tri-nanocomposite in different pHs. Plain DOX was presented for comparison (mean± SD, $n = 3$).

According to Fig. 6a, plain DOX displayed fast release rates of 83% and 70% after 2 h dialysis at pH 5.3 and 7.4, respectively, as previously reported [15].

At the tumor pH of 5.3; a biphasic release pattern was observed (Fig. 6a), with an initial fast release for 4 h, ensuring high DOX concentrations delivered at tumor site, followed by slower release for up to 48 h, with a total of 77.08% of DOX released. Whereas, at physiological pH of 7.4; about 13.60% and 24.50% of DOX was released, after 4 h and 48 h, respectively (Fig. 6a). This result might be due to easier protonation of DOX in lower pH value (i.e. pH 5.3) and hence an increase in its solubility [15]. At lower pH of 5.3, both hydrogen binding and hydrophobic interactions between DOX and the prepared GL-GA-GO nanocomposite were much reduced, leading to DOX quicker release. On the other hand, at pH 7.4, hydrogen binding between DOX and nanocomposite is relatively strong, and the resulting release of DOX is low [15].

As presented in Fig. 6a, a biphasic release pattern of DOX from the nanocomposite was observed at both pHs, which was reported previously [15]. An initial fast release pattern might be due to the presence of available drug near to the surface of nanocomposite, hence promoting its quick diffusion. Whereas, the drug molecules embedded within the composite led to longer travel/diffusion path for the drug, favoring the slow release behavior [15].

It is generally acknowledged that acidic lysosomes reside inside cancer cells [15]. For a successful delivery of any anticancer drug, initially GO allows successful transport of the drug to the cancer cells, followed with drug uptake by the conjugated carriers to the interior of cancer cell via endocytosis. An overall conclusion, DOX can be loaded onto the proposed GL-GA-GO tri-nanocomposite under physiological conditions (pH 7.4) and, alternatively released at reduced, acidic pH of pH 5.3; distinctive of cancerous cells, intracellular lysosomes or endosomes. This phenomenon is quite important in introducing a novel anti-cancer drug delivery system, with enhanced cytotoxic potentials against cancer cells, and minimal adverse effect to normal ones.

Fig. 6b illustrated regression analysis results of different release kinetic models applied to evaluate the biphasic release pattern of DOX from tri-nanocomposite. For both fast release (0–4 h) and slow release (4–48 h) phases; highest values of correlation coefficient were observed for Higuchi square-root of time models, with R2 values of 0.9218 and 0.9886, respectively (Fig. 6b). Meanwhile, upon applying Korsmeyer-Peppas model, values of ´n` parameter were found to be 0.4492 and 0.1968 for the fast and slow release phases, respectively, indicating Fickian diffusion drug release mechanism [45].

Ideal drug release process involves steps of penetration, hydration, dissolution and finally diffusion. In the present study, both gelatin and gum arabic played a dual significant role for stabilizing of GO nanosheets as well as sustaining DOX release from the prepared tri-nanocomposite.

Storage stability of DOX-GL-GA-GO tri-nanocomposite

The prepared DOX loaded nanocomposite was stored in an

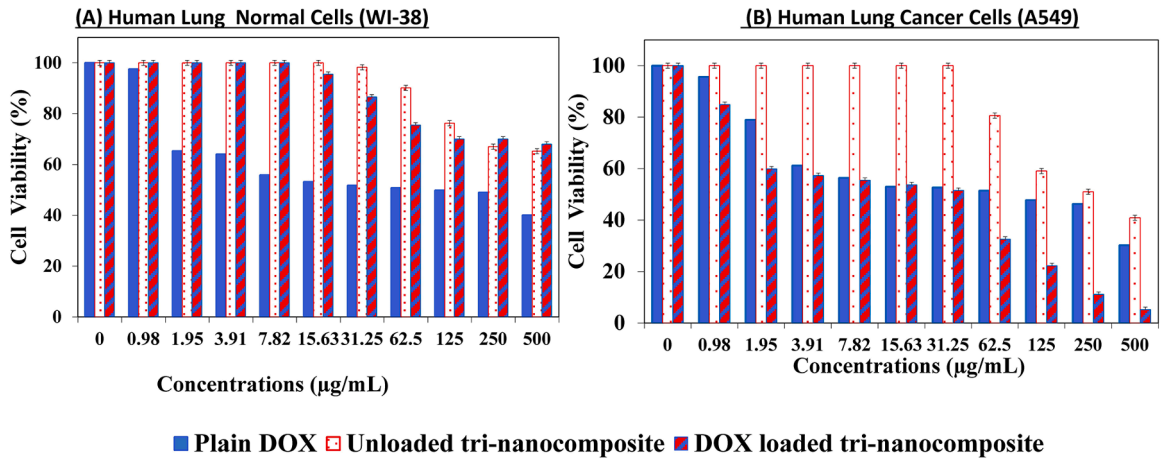

Fig. 7. Cytotoxic activity of un loaded GL-GA-GO composite and DOX loaded composite against plain DOX, in both normal WI-38 lung fibroblast and A549 lung carcinoma cell lines at different concentrations (mean± SD, $n = 3$).

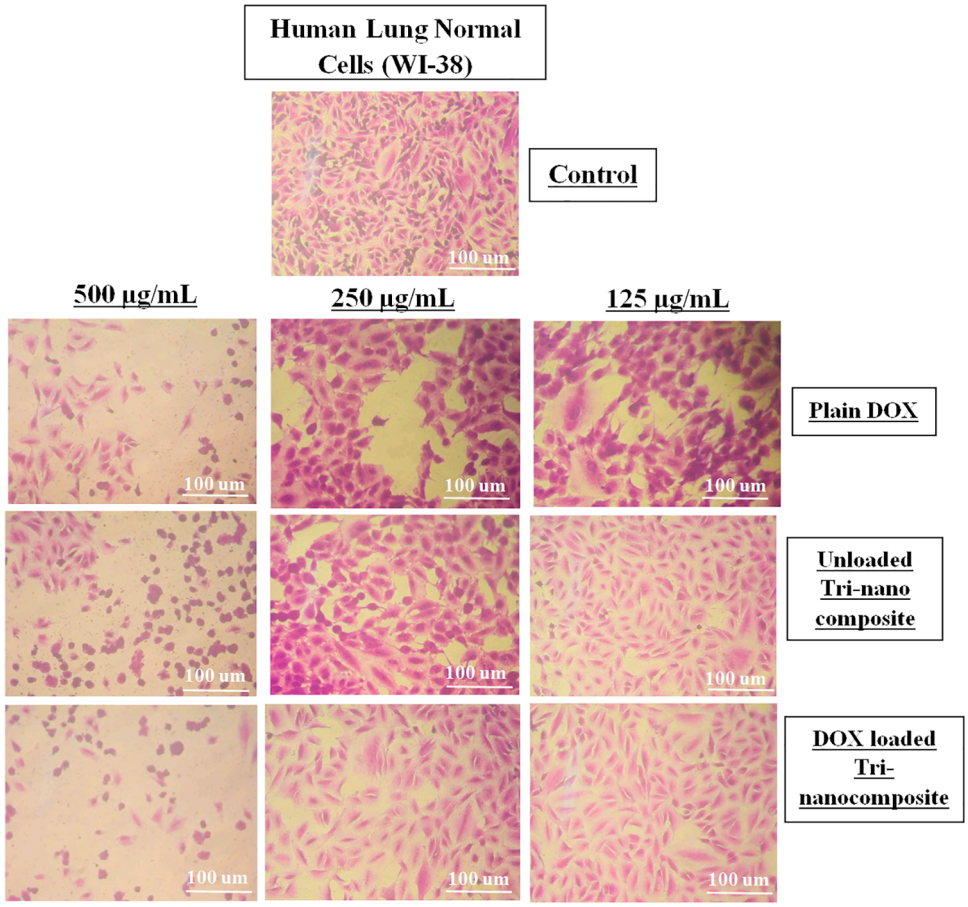

Fig. 8. Inverted microscope images of human lung normal (WI-38) cells treated with plain DOX, unloaded and DOX loaded composite at different concentrations. Magnification: × 40.

accelerated stress environment of 40°C / 75% RH for 3 months. The stored samples were re-evaluated by FTIR, XRD, TEM, zeta potential and in vitro release assays. Physical characteristics of stored loaded nano-composite were comparable with fresh samples as presented by FTIR, TEM and XRD (Supplementary Figure S1), with positive zeta potential value of 15± 1.4 mV. Also, release profile of stored sample was similar with initial data of freshly prepared one, with acceptable f2 value of 75 [69]. These results confirmed the stability of the proposed tri-nanocomposite system over time, which successively enhance its productive usability.

Cytotoxicity results

The most important concerns of using GO for clinical applications, is its compatibility and cellular toxicity. Previous data regarding potential toxic effects of GO is quite conflicting, with some studies confirming low GO cytotoxicity at concentration of 200 µg/mL against A549 cells [70] and WI-38 cells [71], at 100 µg/mL against human fibroblast cells (HDF)

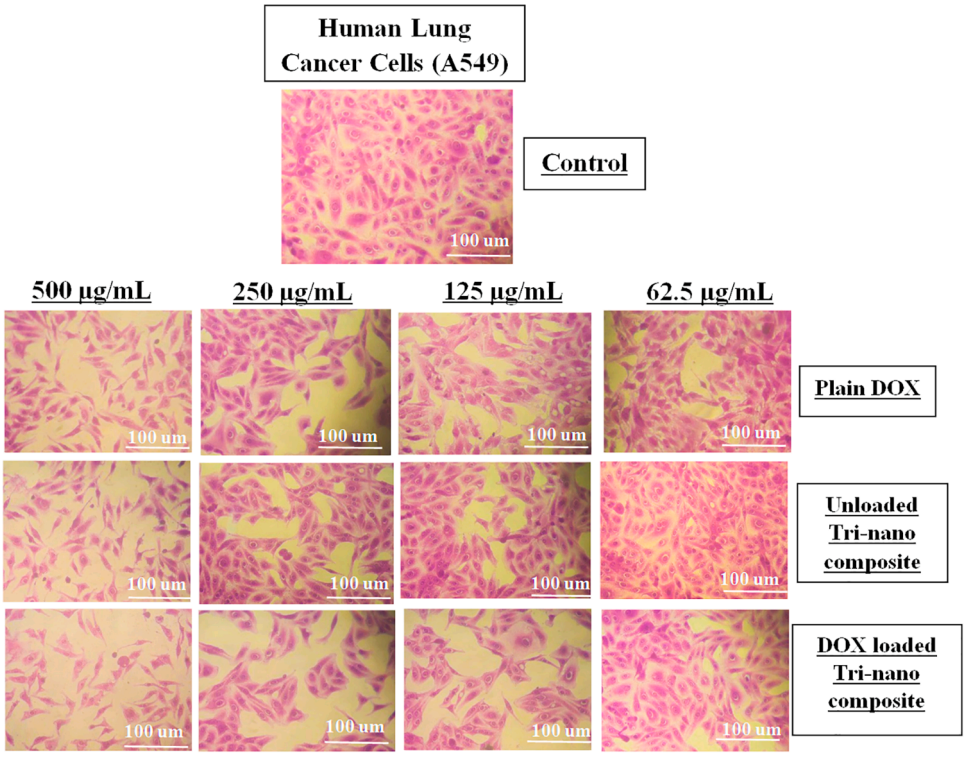

Fig. 9. Inverted microscope images of human lung cancer (A549) cells treated with plain DOX, unloaded and DOX loaded composite at different concentrations. Magnification: × 40.

[72] and at 50 µg/mL against Hela cells [67]. Yet, other reports documented that GO sheets at concentrations above 20 µg/mL induced cytotoxic effects on HDF cells [73], with cytotoxicity reaching 50% for GO concentration of 85 µg/mL against A549 cell line [74]. As reported before, there exist a strong correlation between GO biocompatibility and an increase in its solubility. Functionalization of GO sheets with different biomaterials plays an important role in modulating surface characteristics of GO and its cytotoxic activity [72, 73]. The present study focuses on functionalizing of GL and GA onto GO nanosheets, with the aim of modifying GO toxicity.

The cytotoxic and therapeutic activity of plain DOX, unloaded GL-GA-GO composite as well as DOX loaded composite, in both normal WI-38 lung fibroblast and A549 lung carcinoma cell lines at different concentrations, were expressed as cell viability% (Fig. 7) and IC50. Morphology of WI-38 and A549 under different treatments was illustrated in Figs. 8&9. Control group (with growth media), was set for comparisons.

Evaluation of possible toxicity of the unloaded tri-nanocomposite in both normal and cancer lung cell lines was initially carried out. As depicted from Fig. 7a; No apparent changes in cell viability were observed when WI-38 cells were incubated for 24 h with GL/GA/GO composite having concentrations up to 500 µg/mL, with cell viability value above 65.50%, and an IC50 of 370±1.74. Whereas, reduction of cell viability was observed for A549 cells treated with unloaded tri-nanocomposite, with cell viability value of 40.88% at 500 µg/mL and equivalent IC50 value of 386±0.33 (Fig. 7b).

Both WI-38 and A549 cell lines treated with plain DOX showed marked reduction of cellular activity (Fig. 7), with IC50 reaching 115 ±0.05 and 86±0.42, respectively, which correlate with several previous investigations confirming the powerful chemotherapeutic activity of DOX [21, 70, 73, 75]. However, DOX often undergo early degradation in the biological environment, hence functionalization of DOX with a novel nano-carrier system protect the drug from its degradation and enhance its chemotherapeutic efficiency.

For normal WI-38 lung fibroblast (Fig. 7a); DOX loaded tri-nanocomposite exhibited low cytotoxic effect in comparison with plain DOX with a dose-dependent behavior. At concentration of 31.25 µg/mL; cell viability values of 53.16% and 95.48%, with respective IC50 of 115±0.05 and 185±1.08 ug/mL were recorded for plain DOX and DOX/GL-GA-GO composite samples, respectively.

For A549 lung carcinoma cell line (Fig. 7b); cellular viability was more attenuated for DOX loaded tri-nanocomposite compared with plain drug. A549 cells treated with plain DOX and DOX loaded tri-nanocomposites exhibited IC50 values of 86±0.42 and 51.9 ± 0.46 µg/mL, respectively. Furthermore, the higher inhibition of cancer cell proliferation occurred with the increment of DOX loaded composite's concentration, where DOX/GL-GA-GO with concentrations of 125 and 62.5 µg/mL showed almost 78.34% and 68.87% inhibition of cellular growth. Hence, it could be concluded that the cytotoxic activity of plain DOX was potentiated when loaded onto the tri-nanocomposite.

Morphological observation of WI-38 lung fibroblast under different treatments was illustrated in Fig. 8. Normal WI-38 (control group; with growth medium) exhibited a round, circular structure, identifying regular cellular growth. On the other hand, WI-38 cells treated with plain DOX exhibited apoptosis characteristic including membrane vesicles, fragmentation and undefined cell boundary, with many necrotic areas. These effects were not observed in both unloaded and DOX loaded nanocomposite (Fig. 8).

On the other hand, morphology of A549 cells confirmed reduction in cellular growth after treatment with DOX/GL-GA-GO composite compared to plain DOX (Fig. 9). These results emphasized the efficiency of the prepared drug composite system, where the tri-nanocomposite system successfully decreased the negative cytotoxic effect of plain DOX on normal human cells as well as improved its anticancer activity against lung cancer cells.

In the present study, a tri-nanocomposite is proposed, employing a novel combination of GL/GA and GO with characteristic biocompatibility, nano-size stability as well as targeted DOX delivery into cancer cells. Functionalizing of GL, GA onto GO sheets improved GO physical stability. An initial transport of DOX to cancer cells was done via GO,

followed with targeted drug uptake by the conjugated carriers to the interior of cancer cells via endocytosis. The developed tri-nanocomposite system successfully decreased the negative cytotoxic effect of plain DOX on normal human cells as well as improved its anticancer activity against lung cancer cells.

Conclusion

In the present study, a novel tri-nanocomposite was fabricated, combining the unique properties of biodegradable GL, GA and GO for improved cancer treatment efficacy. The prepared nontoxic and biocompatible nanocomposite system of GL/GA functionalized onto GO mono sheets was employed for efficient loading and controlling the release of an anti-cancer model drug, DOX. Developed tri-nanocomposite showed good biocompatibility, nano-size stability as well as high DOX loading. DOX release performance from loaded composite was pH-sensitive, with faster release rate in cancerous pH, compared to physiological pH. The prepared unloaded tri-nanocomposite exhibited no cytotoxicity to both WI-38 and A549 cells. High antitumor activity of DOX loaded nanocomposite was observed in comparison with plain DOX, with IC_{50} values of 51.9 ± 0.46 and 86.6 ± 0.42 μg/mL, respectively against A549 cells. Additionally, DOX loaded composite exhibited less toxicity to normal WI-38 cells compared to plain DOX, with equivalent IC_{50} values of 185±1.08 and 115±0.046 μg/mL, respectively.

Statement of informed consent

Informed consent was obtained from all individual participants included in the study.

Declaration of conflicts of interest

The authors report no conflicts of interest in this work.

Supplementary materials

Supplementary material associated with this article can be found, in the online version, at doi:10.1016/j.btre.2022.e00722.

References

[1] S. Zhou, Q. Shang, N. Wang, Q. Li, A. Song, Y. Luan, Rational design of a minimalist nanoplatform to maximize immunotherapeutic efficacy: four birds with one stone, J Control Release. Dec 10, 328 (2020) 617–630.

[2] N. Hazhir, F. Chekin, J. Raoof, S. Fathi, A porous reduced graphene oxide/chitosan-based nanocarrier as a delivery system of doxorubicin, RSC Adv. 9 (2019) 30729–30735.

[3] M. Zhang, X. Qin, W. Xu, Y. Wang, Y. Song, S. Garg, Y. Luan, Engineering of a dual-modal phototherapeutic nanoplatform for single NIR laser-triggered tumor therapy, J. Colloid Interface Sci. 594 (2021) 493–501.

[4] C. Wang, Z. Zhang, B. Chen, L. Gu, Y. Li, S. Yu, Design and evaluation of galactosylated chitosan/graphene oxide nanoparticles as a drug delivery system, J. Colloid Interface Sci. 516 (2018) 332–341.

[5] Y. Lu, W. Sun, Z. Gu, Stimuli-responsive nanomaterials for therapeutic protein delivery, J. Control. Release. 194 (2014) 1–19.

[6] M. Zhang, X. Qin, Z. Zhao, Q. Du, Q. Li, Y. Jiang, Y. Luan, A self-amplifying nanodrug to manipulate the Janus-faced nature of ferroptosis for tumor therapy, Nanoscale Horiz 7 (2022) 198–210.

[7] H. Namazi, Polymers in our daily life, BioImpacts: BI 7 (2017) 73.

[8] J.S. Son, M. Appleford, J.L. Ong, J.C. Wenke, J.M. Kim, S.H. Choi, D.S. Oh, Porous hydroxyapatite scaffold with three-dimensional localized drug delivery system using biodegradable microspheres, J. Control. Release. 153 (2011) 133–140.

[9] H. Namazi, M. Adeli, Dendrimers of citric acid and poly (ethylene glycol) as the new drug-delivery agents, Biomaterials 26 (2005) 1175–1183.

[10] S.A. Abraham, D.N. Waterhouse, L.D. Mayer, P.R. Cullis, T.D. Madden, M.B. Bally, The liposomal formulation of doxorubicin, Methods Enzymol. 391 (2005) 71–97.

[11] M.S. Hasanin, M. Abdelraof, M. Fikry, Y.M. Shaker, A.M. Sweed, M.O. Senge, Development of Antimicrobial Laser-Induced Photodynamic Therapy Based on Ethylcellulose/Chitosan Nanocomposite with 5, 10, 15, 20-Tetrakis (m-Hydroxyphenyl) porphyrin, Molecules 26 (2021) 3551.

[12] H. Ilkhani, T. Hughes, J. Li, C.J. Zhong, M. Hepel, Nanostructured SERS-electrochemical biosensors for testing of anticancer drug interactions with DNA, Biosens. Bioelectron. 80 (2016) 257–264.

[13] A.H. Hashem, M. Hasanin, S. Kamel, S.J.C. Dacrory, S.B. Biointerfaces, A new approach for antimicrobial and antiviral activities of biocompatible nanocomposite based on cellulose, Amino Acid and Graphene Oxide (2021), 112172.

[14] L. Anchique, J.J. Alcázar, A. Ramos-Hernandez, M. Méndez-López, J.R. Mora, N. Rangel, J.L. Paz, E. Márquez, Predicting the Adsorption of Amoxicillin and Ibuprofen on Chitosan and Graphene Oxide Materials: a Density Functional Theory Study, Polymers (Basel) 13 (2021) 1620.

[15] B. Zhang, X. Yang, Y. Wang, G. Zhai, Heparin modified graphene oxide for pH-sensitive sustained release of doxorubicin hydrochloride, Mater. Sci. Eng. C 75 (2017) 198–206.

[16] L. Asadi, S. Shirvalilou, S. Khoee, S. Khoei, Cytotoxic effect of 5-fluorouracil-loaded polymer-coated magnetite nanographene oxide combined with radiofrequency, Anti-Cancer Agents Med. Chem. 18 (2018) 1148–1155.

[17] D. de Melo-Diogo, E.C. Costa, C.G. Alves, R. Lima-Sousa, P. Ferreira, R.O. Louro, I. J. Correia, POxylated graphene oxide nanomaterials for combination chemo-phototherapy of breast cancer cells, Eur. J. Pharm. Biopharm. 131 (2018) 162–169.

[18] M.H. Zainal-Abidin, M. Hayyan, G.C. Ngoh, W.F. Wong, Doxorubicin loading on functional graphene as a promising nanocarrier using ternary deep eutectic solvent systems, ACS Omega 5 (2020) 1656–1668.

[19] Z. Liu, J.T. Robinson, X. Sun, H. Dai, PEGylated nanographene oxide for delivery of water-insoluble cancer drugs, J. Am. Chem. Soc. 130 (2008) 10876–10877.

[20] S. Wu, X. Zhao, Y. Li, Q. Du, J. Sun, Y. Wang, X. Wang, Y. Xia, Z. Wang, L. Xia, Adsorption properties of doxorubicin hydrochloride onto graphene oxide: equilibrium, kinetic and thermodynamic studies, Materials (Basel) 6 (2013) 2026–2042.

[21] S. Zhang, K. Yang, L. Feng, Z. Liu, In vitro and in vivo behaviors of dextran functionalized graphene, Carbon N Y 49 (2011) 4040–4049.

[22] J. An, Y. Gou, C. Yang, F. Hu, C. Wang, Synthesis of a biocompatible gelatin functionalized graphene nanosheets and its application for drug delivery, Mater. Sci. Eng. C 33 (2013) 2827–2837.

[23] A. Shehabeldine, H. El-Hamshary, M. Hasanin, A. El-Faham, M.J.P. Al-Sahly, Enhancing the antifungal activity of griseofulvin by incorporation a green biopolymer-based, Nanocomposite 13 (2021) 542.

[24] C. Wan, M. Frydrych, B. Chen, Strong and bioactive gelatin–graphene oxide nanocomposites, Soft Matter 7 (2011) 6159–6166.

[25] N.S. El-Sayed, A.H. Hashem, S. Kamel, Preparation and characterization of Gum Arabic Schiff's bases based on 9-aminoacridine with in vitro evaluation of their antimicrobial and antitumor potentiality, Carbohydr. Polym. 277 (2022), 118823.

[26] G.O. Phillips, Molecular association and function of arabinogalactan protein complexes from tree exudates, Struct. Chem. 20 (2009) 309–315.

[27] E. Dickinson, Hydrocolloids at interfaces and the influence on the properties of dispersed systems, Food Hydrocoll 17 (2003) 25–39.

[28] A.C. Roque, A. Bicho, I.L. Batalha, A.S. Cardoso, A. Hussain, Biocompatible and bioactive gum Arabic coated iron oxide magnetic nanoparticles, J. Biotechnol. 144 (2009) 313–320.

[29] R. Bandyopadhyaya, E. Nativ-Roth, O. Regev, R. Yerushalmi-Rozen, Stabilization of individual carbon nanotubes in aqueous solutions, Nano Lett. 2 (2002) 25–28.

[30] M. Thakur, S. Pandey, A. Mewada, R. Shah, G. Oza, M. Sharon, Understanding the stability of silver nanoparticles bio-fabricated using Acacia arabica (Babool gum) and its hostile effect on microorganisms, Spectrochim. Acta A Mol. Biomol. Spectrosc. 109 (2013) 344–347.

[31] D. Rana, B.M. Mandal, S.N. Bhattacharyya, Miscibility and phase diagrams of poly (phenyl acrylate) and poly (styrene-co-acrylonitrile) blends, Polymer (Guildf) 34 (7) (1993) 1454–1459.

[32] D. Rana, B.M. Mandal, S.N. Bhattacharyya, Analogue calorimetry of polymer blends: poly (styrene-co-acrylonitrile) and poly (phenyl acrylate) or poly (vinyl benzoate), Polymer (Guildf) 37 (12) (1996) 2439–2443.

[33] D. Rana, K. Bag, S.N. Bhattacharyya, B.M. Mandal, Miscibility of poly (styrene-co-butyl acrylate) with poly (ethyl methacrylate): existence of both UCST and LCST, J. Polymer Sci. Part B: Polymer Physics. 38 (3) (2000) 369–375.

[34] D. Rana, B.M. Mandal, S.N. Bhattacharyya, Analogue calorimetric studies of blends of poly (vinyl ester) s and polyacrylates, Macromolecules 29 (5) (1996) 1579–1583.

[35] V.Y. Grinberg, V. Tolstoguzov, Thermodynamic incompatibility of proteins and polysaccharides in solutions, Food Hydrocoll 11 (2) (1997) 145–158.

[36] F.A. Fornari, J.K. Randolph, J.C. Yalowich, M.K. Ritke, D.A. Gewirtz, Interference by doxorubicin with DNA unwinding in MCF-7 breast tumor cells, Mol. Pharmacol. 45 (1994) 649–656.

[37] J. You, G. Zhang, C. Li, Exceptionally high payload of doxorubicin in hollow gold nanospheres for near-infrared light-triggered drug release, ACS Nano 4 (2010) 1033–1041.

[38] E. Quagliarini, R. Di Santo, D. Pozzi, P. Tentori, F. Cardarelli, G. Caracciolo, Mechanistic Insights into the Release of Doxorubicin from Graphene Oxide in Cancer Cells, Nanomaterials 10 (2020) 1482.

[39] M.S. Khan, S. Pandey, M.L. Bhaisare, G. Gedda, A. Talib, .H..-F. Wu, Graphene oxide@ gold nanorods for chemo-photothermal treatment and controlled release of doxorubicin in mice Tumor, Colloids Surf. B: Biointerfaces. 160 (2017) 543–552.

[40] W.S. Hummers Jr, R.E. Offeman, Preparation of graphitic oxide, J. Am. Chem. Soc. 80 (1958) 1339. -1339.

[41] C. Xu, D. Yang, L. Mei, Q. Li, H. Zhu, T. Wang, Targeting chemophotothermal therapy of hepatoma by gold nanorods/graphene oxide core/shell nanocomposites, ACS Appl. Mater. Interfaces 5 (2013) 12911–12920.

[42] A. Sood, R. Panchagnula, Drug release evaluation of diltiazem CR preparations, Int. J. Pharm. 175 (1998) 95–107.
[43] M.R. Wright, Introduction to Chemical Kinetics, John Wiley & Sons, Chichester, England, 2004.
[44] E. Karasulu, H.Y. Karasulu, G. Ertan, L. Kirilmaz, T. Güneri, Extended release lipophilic indomethacin microspheres: formulation factors and mathematical equations fitted drug release rates, Eur. J. Pharm. Sci. 19 (2003) 99–104.
[45] R.W. Korsmeyer, R. Gurny, E. Doelker, P. Buri, N.A. Peppas, Mechanisms of solute release from porous hydrophilic polymers, Int. J. Pharm. 15 (1983) 25–35.
[46] N. Taha, K. Mahmoud, A. Soliman, L. Emara, Anti-inflammatory and cytoprotective potentials of Meloxicam solid dispersions prepared by different techniques on lipopolysaccharide-stimulated RAW 264.7 macrophages, J. Drug Deliv. Sci. Technol. 63 (2021), 102507.
[47] Y.-.L. Cheng, W.-.L. Chang, S.-.C. Lee, Y.-.G. Liu, H.-.C. Lin, C.-.J. Chen, C.-.Y. Yen, D.-.S. Yu, S.-.Z. Lin, .H..-J. Harn, Acetone extract of Bupleurum scorzonerifolium inhibits proliferation of A549 human lung cancer cells via inducing apoptosis and suppressing telomerase activity, Life Sci. 73 (2003) 2383–2394.
[48] T. Anirudhan, V.C. Sekhar, V. Athira, Graphene oxide based functionalized chitosan polyelectrolyte nanocomposite for targeted and pH responsive drug delivery, Int. J. Biol. Macromol. 150 (2020) 468–479.
[49] Z. Liu, J. Liu, T. Wang, Q. Li, P.S. Francis, C.J. Barrow, W. Duan, W. Yang, Switching off the interactions between graphene oxide and doxorubicin using vitamin C: combining simplicity and efficiency in drug delivery, J. Mater. Chem. B. 6 (2018) 1251–1259.
[50] T. Mahendran, P.A. Williams, G.O. Phillips, S. Al-Assaf, T.C. Baldwin, New insights into the structural characteristics of the arabinogalactan−protein (AGP) fraction of gum Arabic, J. Agric. Food Chem. 56 (2008) 9269–9276.
[51] A. Rahdar, M.R. Hajinezhad, H. Hamishekar, A. Ghamkhari, G.Z. Kyzas, Copolymer/graphene oxide nanocomposites as potential anticancer agents, Polym. Bull. 78 (2021) 4877–4898.
[52] N. Meng, Y. Su, N. Zhou, M. Zhang, M. Shao, Y. Fan, H. Zhu, P. Yuan, C. Chi, Y. Xiao, Carboxylated graphene oxide functionalized with β-cyclodextrin—Engineering of a novel nanohybrid drug carrier, Int. J. Biol. Macromol. 93 (2016) 117–122.
[53] S. Syama, C. RS, A.C. Poulose, T. Maekawa, D. Sakthikumar, P.V. Mohanan, Synthesis and characterization of pegylated reduced graphene oxide: determination of toxicity using bone marrow mesenchymal stem cells, J. Appl. Chem. Sci. Int. 5 (2016) 1–11.
[54] S. Jalili-Firoozinezhad, M.H. Mohamadzadeh Moghadam, M.H. Ghanian, M. K. Ashtiani, H. Alimadadi, H. Baharvand, I. Martin, A. Scherberich, Polycaprolactone-templated reduced-graphene oxide liquid crystal nanofibers towards biomedical applications, RSC Adv. 7 (2017) 39628–39634.
[55] M. Bashir, S. Haripriya, Assessment of physical and structural characteristics of almond gum, Int. J. Biol. Macromol. 93 (2016) 476–482.
[56] B. Gaihre, Y. Hee Lee, M. Seob Khil, H. Keun Yi, H. Yong Kim, In-vitro cytotoxicity and cell uptake study of gelatin-coated magnetic iron oxide nanoparticles, J. Microencapsul. 28 (2011) 240–247.
[57] R. Bansal, R. Singh, K. Kaur, Quantitative analysis of doxorubicin hydrochloride and arterolane maleate by mid IR spectroscopy using transmission and reflectance modes, BMC Chem 15 (2021) 1–11.
[58] W.J. Fávaro, J.G. de Souza, L.A. Ferreira, M.B. de Jesus, M. Durán, P. K. Bockelmann, J.S. Bernardes, N. Durán, Hybrid graphene oxide as carrier of doxorubicin: cytotoxicity and preliminary in vivo assays against bladder cancer, Adv. Nat. Sci.: Nanosci. Nanotechnol. 11 (2020), 025016.
[59] Y. Bernal, J. Alvarado, R. Juárez, E. de Vasconcelos, W. de Azevedo, B.-.S. Soto-Cruz, Synthesis and characterization of carbon nanotubes/silica composites using gum arabic, Mater. Res. Express. 5 (2018), 075028.
[60] K. Pal, A.K. Banthia, D.K. Majumdar, Preparation and characterization of polyvinyl alcohol-gelatin hydrogel membranes for biomedical applications, AAPS Pharm. Sci. Tech 8 (2007) E142–E146.
[61] X. Zhao, Q. Chen, W. Liu, Y. Li, H. Tang, X. Liu, X. Yang, Codelivery of doxorubicin and curcumin with lipid nanoparticles results in improved efficacy of chemotherapy in liver cancer, Int. J. Nanomed. 10 (2015) 257.
[62] K.-.W. Park, J.H. Jung, Spectroscopic and electrochemical characteristics of a carboxylated graphene–ZnO composites, J. Power Sources 199 (2012) 379–385.
[63] H.-.W. Yang, M.-.Y. Hua, S.-.L. Chen, .R..-Y. Tsai, Reusable sensor based on high magnetization carboxyl-modified graphene oxide with intrinsic hydrogen peroxide catalytic activity for hydrogen peroxide and glucose detection, Biosens. Bioelectron. 41 (2013) 172–179.
[64] D. Depan, J. Shah, R. Misra, Controlled release of drug from folate-decorated and graphene mediated drug delivery system: synthesis, loading efficiency, and drug release response, Mater. Sci. Eng. C 31 (2011) 1305–1312.
[65] A. Kumar, C.K. Dixit, Methods for characterization of nanoparticles, in: S. Nimesh, R. Chandra, N. Gupta (Eds.), Advances in Nanomedicine for the Delivery of Therapeutic Nucleic Acids, Woodhead Publishing, Sawston, CA, USA, 2017, pp. 43–58.
[66] W. Chen, F. Meng, R. Cheng, Z. Zhong, pH-Sensitive degradable polymersomes for triggered release of anticancer drugs: a comparative study with micelles, J. Control. Release. 142 (2010) 40–46.
[67] X. Yang, Y. Wang, X. Huang, Y. Ma, Y. Huang, R. Yang, H. Duan, Y. Chen, Multi-functionalized graphene oxide based anticancer drug-carrier with dual-targeting function and pH-sensitivity, J. Mater. Chem. 21 (2011) 3448–3454.
[68] X. Yang, X. Zhang, Z. Liu, Y. Ma, Y. Huang, Y. Chen, High-efficiency loading and controlled release of doxorubicin hydrochloride on graphene oxide, J. Phys. Chem. C. 112 (2008) 17554–17558.
[69] J.W. Moore, H.H. Flanner, Mathematical comparison of dissolution profiles, Pharm. Technol. 20 (1996) 64–74.
[70] Y. Chang, S.-.T. Yang, J.-.H. Liu, E. Dong, Y. Wang, A. Cao, Y. Liu, H. Wang, In vitro toxicity evaluation of graphene oxide on A549 cells, Toxicol. Lett. 200 (2011) 201–210.
[71] A.M. Sawy, A. Barhoum, S.A.A. Gaber, S.M. El-Hallouty, W.G. Shousha, A. A. Maarouf, A.S. Khalil, Insights of doxorubicin loaded graphene quantum dots: synthesis, DFT drug interactions, and cytotoxicity, Mater. Sci. Eng. C 122 (2021), 111921.
[72] K.-.H. Liao, Y.-.S. Lin, C.W. Macosko, C.L. Haynes, Cytotoxicity of graphene oxide and graphene in human erythrocytes and skin fibroblasts, ACS Appl. Mater. Interfaces 3 (2011) 2607–2615.
[73] K. Wang, J. Ruan, H. Song, J. Zhang, Y. Wo, S. Guo, D. Cui, Biocompatibility of graphene oxide, Nanoscale Res. Lett. 6 (2011) 1–8.
[74] W. Hu, C. Peng, W. Luo, M. Lv, X. Li, D. Li, Q. Huang, C. Fan, Graphene-based antibacterial paper, ACS Nano 4 (2010) 4317–4323.
[75] M.S. Hasanin, M. El-Sakhawy, H.Y. Ahmed, S. Kamel, Hydroxypropyl methylcellulose/graphene oxide composite as drug carrier system for5-Fluorouracil, Biotechnol. J. (2021), 2100183.